**Atmospheric
Chemistry
and Physics
Discussions**

Atmospheric three-dimensional inverse modeling of regional industrial emissions and global oceanic uptake of carbon tetrachloride

X. Xiao[1,*], R. G. Prinn[1], P. J. Fraser[2], R. F. Weiss[3], P. G. Simmonds[4],
S. O'Doherty[4], B. R. Miller[5], P. K. Salameh[3], C. M. Harth[3], P. B. Krummel[2],
A. Golombek[1], L. W. Porter[6,†], J. W. Elkins[5], G. S. Dutton[5], B. D. Hall[5],
L. P. Steele[2], R. H. J. Wang[7], and D. M. Cunnold[7,†]

[1]Department of Earth, Atmospheric, and Planetary Sciences, MIT, Cambridge, MA 02139, USA
[2]Centre for Australian Weather and Climate Research, CSIRO Marine and Atmospheric Research, Aspendale, Victoria 3195, Australia
[3]Scripps Institution of Oceanography, University of California, San Diego, La Jolla, CA 92093, USA
[4]School of Chemistry, University of Bristol, Bristol, UK
[5]ESRL, NOAA, Boulder, CO 80305, USA

Title Page

Abstract	Introduction
Conclusions	References
Tables	Figures

|◄ | ►|

◄ | ►

Back | Close

Full Screen / Esc

Printer-friendly Version

Interactive Discussion

[6] Centre for Australian Weather and Climate Research, Australian Government Bureau of Meteorology, Melbourne, Victoria 3000, Australia

[7] School of Earth and Atmospheric Sciences, Georgia Institute of Technology, Atlanta, GA 30332, USA

[*] now at: Civil & Environmental Engineering, Rice University, Houston, TX 77005, USA

[†] deceased

Correspondence to: X. Xiao (xue.xiao@rice.edu)

Discussion Paper | Discussion Paper | Discussion Paper | Discussion Paper |

Abstract

Carbon tetrachloride (CCl_4) has substantial stratospheric ozone depletion potential and its consumption is controlled under the Montreal Protocol and its amendments. We implement a Kalman filter using atmospheric $CC1_4$ measurements and a 3-dimensional chemical transport model to estimate the interannual regional industrial emissions and seasonal global oceanic uptake of CCl_4 for the period of 1996–2004. The Model of Atmospheric Transport and Chemistry (MATCH), driven by offline National Center for Environmental Prediction (NCEP) reanalysis meteorological fields, is used to simulate CCl_4 mole fractions and calculate their sensitivities to regional sources and sinks using a finite difference approach. High frequency observations from the Advanced Global Atmospheric Gases Experiment (AGAGE) and NOAA Earth System Research Laboratory (ESRL) and low frequency flask observations are together used to constrain the source and sink magnitudes, estimated as factors that multiply the a priori fluxes. Although industry data imply that the global industrial emissions were substantially declining with large interannual variations, the optimized results show only small interannual variations and a small decreasing trend. The global surface CCl_4 mole fractions were declining in this period because the CCl_4 oceanic and stratospheric sinks exceeded the industrial emissions. Compared to the a priori values, the inversion results indicate substantial increases in industrial emissions originating from the South Asian/Indian and Southeast Asian regions, and significant decreases in emissions from the European and North American regions.

1 Introduction

Global carbon tetrachloride (CCl_4) consumption is controlled by the Montreal Protocol and its various amendments due to its long lifetime (about 26 years) and large Ozone Depletion Potential (0.73 relative to 1.0 for CFC-11) (Montzka et al., 2003). It is also a greenhouse gas with a Global Warming Potential of 1380 (compared to 1.0 for CO_2)

on a 100-year time frame (Montzka et al., 2003). Carbon tetrachloride in the atmosphere originates almost exclusively from fugitive emissions from its industrial uses (Simmonds et al., 1998), although there may be a small natural source (Butler et al., 1999). The current 2009 global average tropospheric dry-air mole fraction of CCl_4 is $\sim$87 ppt (parts per trillion), while historically, concentrations of CCl_4 reached a peak value of $\sim$105 ppt in 1990 (Montzka et al., 1996, 1999; Simmonds et al., 1998; Prinn et al., 2000). The decrease in its global average mole fraction has largely resulted from the emissions reductions achieved under the Montreal Protocol. The CCl_4 mole fraction in the Northern Hemisphere (NH) has been about 2% higher than in the Southern Hemisphere (SH) fairly steadily since 1993, which indicates that significant emissions of CCl_4 still remain today (Montzka et al., 2003).

The principal identified uses of CCl_4 are as a general purpose solvent and also, since 1931, as a feedstock for the production of CFC-11 (CCl_3F), CFC-12 (CCl_2F_2) and other chlorofluorocarbons (CFCs). Releases to the atmosphere from this CFC production arise only from fugitive losses (Montzka et al., 2003). Large discrepancies have existed in United Nations Environment Program (UNEP) production and consumption data for past years owing in part to confusion over reporting procedures and this has led to significant omissions and/or underestimates of CCl_4 emissions (Montzka et al., 2003). Therefore CCl_4 fugitive emission estimates have been derived indirectly by using CFC-11 and CFC-12 production as proxies (Cunnold et al., 1997; Simmonds et al., 1998). The principal sink for CCl_4 is stratospheric photodissociation, which is known to produce phosgene (Kindler et al., 1995). Using an assumed partial atmospheric lifetime (global mass divided by stratospheric mass loss rate) of $\sim$42 years, and atmospheric measurements from 1978–1996, Simmonds et al. (1998) implemented an inverse method with a 2-dimensional (2-D) model to estimate that the global CCl_4 emissions averaged around 94 Gg yr^{-1} for 1979–1988 and 49 Gg yr^{-1} for 1991–1995. Using stratospheric observations, and assuming that destruction in the stratosphere is the ultimate sink of CCl_4 (Volk et al., 1997), it has been suggested that a more accurate estimate of the stratospheric partial lifetime is 35 years (Prinn et al., 1999). This is also

X. Xiao et al.

Title Page

Abstract | Introduction

Conclusions | References

Tables | Figures

◄ | ►

◄ | ►

Back | Close

Full Screen / Esc

Printer-friendly Version

Interactive Discussion

in good agreement with the lifetime of 34±5 years recently deduced from the Atmospheric Chemistry Experiment (ACE) data (Allen et al., 2009). The oceans have also been quantified as a global sink of CCl_4 with a partial atmospheric lifetime of 94 years (Yvon-Lewis and Butler, 2002), which lowers the total atmospheric lifetime to 26 years when combined inversely with the above 35-year stratospheric partial lifetime (Montzka et al., 2003). This updated estimate of the total lifetime implies that the global emissions of CCl_4 had been previously underestimated. More recently soils have also been proposed to be a global sink of CCl_4 that is even stronger than the oceanic sink (Happell and Roche, 2003). This additional identified sink would lower the total lifetime of CCl_4 to 20 years. However, the measured inter-hemispheric gradient of CCl_4 appears to be inconsistent with inclusion of a soil sink (dominated by the NH) and an overall lifetime of 20 years. Therefore the lifetime of 26 years is still recommended (Clerbaux et al., 2007).

Given the difficulties and discrepancies in the "bottom-up" approaches (UNEP, CFC scaling) for estimating CCl_4 production, consumption, and fugitive emissions, the objectives of this work are to optimally deduce CCl_4 industrial emissions using a "top-down" or inverse modeling approach. Previous inversions with 2-D models could not be used to estimate the regional distributions of CCl_4 emissions that are expected to change over time because the Montreal Protocol has significant variations in mandated reductions from one region to another. In the work reported here, we estimate the magnitudes of the industrial emissions from eight global land regions and also the global oceanic sink of CCl_4 using a global 3-dimensional (3-D) model, global CCl_4 observations and a discrete Kalman filter. Interannual variability of the above industrial land sources and intra-annual and interannual variability of the oceanic sink is solved as individual 12-month and 3-month pulses in the inverse modeling. Descriptions of the observations and 3-D chemical transport model are given in Sect. 2. The inverse methodology is presented in Sect. 3, and the inversion results and final conclusions are given in Sects. 4 and 5, respectively.

2 Observations and the model

2.1 Atmospheric observations of CCl$_4$

This study uses observations of CCl$_4$ from the in situ high frequency stations of the NASA Advanced Global Atmospheric Gases Experiment (AGAGE; gas chromatographs with electron capture detection) (Prinn et al., 2000) and the NOAA Earth Systems Research Laboratory (ESRL) networks (ftp://ftp.cmdl.noaa.gov/hats/solvents/CCl4/insituGCs/). Low frequency flask observations from NOAA-ESRL stations are also utilized (ftp://ftp.cmdl.noaa.gov/hats/solvents/CCl4/Flasks/Otto/monthly/). Figure 1 shows the locations of these surface measurement sites, and other relevant information about them is given in Table 1.

The two measuring networks use different and independent calibration standards, and their data need to be converted to the same calibration scale when combined together and used in the inversions. Regular inter-comparisons of AGAGE and ESRL observations provide the ratios of the ESRL to AGAGE data at common sites (Krummel et al., 2008). Then the ratios are averaged to determine the typical calibration ratios of the ESRL to AGAGE standards (Table 1). In this work we convert the data on ESRL scale to be expressed on the AGAGE scale. Note that the scales differ by only about 3% and that an equally valid choice would be to place all the data on the ESRL scale.

One advantage of the Kalman filter is that it weights the optimal solutions by accounting for the uncertainties in both the observations and the a priori emission estimates. The uncertainties in the observed mole fractions, and the sensitivity of emission updates to changes in these mole fractions, jointly determine their usefulness in deducing the optimized results (Prinn, 2000). For estimating annual and seasonal surface fluxes it is adequate to utilize monthly mean CCl$_4$ mole fractions (χ) and their associated uncertainties expressed as standard errors (denoted σ) under the assumption of a normal distribution. In general the monthly means are derived as the average of the measurements made at each site for each month omitting periods of obvious pollution. The variances of the uncertainties (σ^2) have three components associated with the

Full Screen / Esc

Printer-friendly Version

Interactive Discussion

instrumental error, the sampling frequency error, and the so-called mismatch or representation error. The methodology for derivation of the monthly mean mole fractions and variances of their uncertainties for both high frequency in situ and low frequency flask measurements is described in detail in a companion paper for methyl chloride (CH$_3$Cl, Xiao et al., 2009), which is based in turn upon a previous inverse study estimating methane (CH$_4$) emissions (Chen and Prinn, 2006).

2.2 The 3-D chemical transport model

The 3-D Model of Atmospheric Transport and Chemistry (MATCH) (Rasch et al., 1997; Mahowald, 1996; Mahowald et al., 1997a, b) is used in this work to simulate the global 3-D distributions of the mole fractions of CCl$_4$. The model is driven by National Center for Environmental Prediction (NCEP) assimilated meteorology. The chosen horizontal resolution of the model is T42, corresponding to approximately 2.8$°\times$ 2.8$°$ (64$\times$128 grid points). There are 28 sigma levels in the vertical direction. The model time step is 40 minutes, and these high frequency outputs are then averaged to derive modeled monthly means at the grid cells containing the observing stations.

In the stratosphere, CCl$_4$ is photodissociated and oxidized by O^1(D). Stratospheric photodissociation is its most important sink, and is much larger than the destruction by O^1(D) (Golombek and Prinn, 1986, 1989, 1993). The chemical destruction rates (J values in s^{-1}) for stratospheric photodissociation of CCl$_4$ have been calculated from a more detailed 3-D model for the stratosphere (Golombek and Prinn, 1986, 1989, 1993, updated here with the latest kinetic and photolysis data). Here we interpolate the monthly mean photodissociation rate fields that vary with latitude and altitude from the stratospheric model grids to the MATCH grids. We do not explicitly model stratospheric destruction of CCl$_4$ by O^1(D) since it is minor, as mentioned above. The J values are then modified by a constant global factor to reflect the appropriate best estimate of the stratospheric lifetime for CCl$_4$, which is ~35 years as noted earlier. Due to interpolation errors associated with the very rapid increase of the J values in the vertical direction in the stratosphere, and the somewhat overestimated stratosphere-

troposphere exchange (STE) rate in MATCH (Jöckel et al., 2002), the stratospheric sink was actually overestimated in the initial trial run and had to be adjusted downwards to yield the 35-year lifetime. To do the adjustment, we first run the forward model for four years from 1992 to 1995, and then calculate the implied stratospheric lifetime

5 and then decrease the J values appropriately. This process is iterated until we get the desired lifetime. We finally calculate the stratospheric lifetime for the whole period of interest from 1996 to 2005 and make needed final adjustment to ensure that the time-averaged stratospheric lifetime is ~35 years.

3   Methodology for inverse modeling

10 To estimate the surface fluxes of CCl$_4$ industrial sources and the oceanic sink and their uncertainties, we use the discrete Kalman filter, which has been adapted here to estimate time-varying flux magnitudes at either 12-month or 3-month time resolution on regional or global scales. Details concerning implementation and interpretation of the Kalman filter can be found in Prinn (2000). We estimate the spatially integrated flux

15 magnitudes for several defined regions of the world, with the flux patterns within them being prescribed. Specifically we estimate factors multiplying the a priori reference magnitudes for the surface fluxes, because the magnitudes of the fluxes themselves differ by orders of magnitude that can lead to near-singular matrices in numerical computations. Also, for this Eulerian chemical transport model, we specifically calculate

20 adjustments to the reference mole fractions and fluxes (Prinn, 2000).

Reference (a priori) flux distributions are necessary to initialize the Kalman filter and to calculate the sensitivities of CCl$_4$ mole fractions to the surface flux magnitudes. As noted in the introduction, there have been previous estimates of CCl$_4$ industrial emissions from industrial sales data and from inversions using a 2-D model. Figure 2 shows

25 the yearly global industrial emission estimates from industrial sales data (McCulloch, private communication, 2009) and the estimates from the 2-D model inverse modeling approach applied only to AGAGE data (Cunnold et al., 1997; Simmonds et al., 1998)

updated to 2004. Also shown are the corresponding linearly fitted lines. Note that there are two quasi-linear regimes in the 2-D model emission estimates, and the linearly fitted yearly global emissions for the 1996–2004 regime are used as our a priori or reference values.

For the a priori spatial distributions of CCl$_4$ industrial sources, the above global emissions were subdivided country-by-country based on gross domestic product (GDP). Population density was then used as a spatial proxy for emissions within countries. This approach produces a map that would be most appropriate for countries prior to substantial reductions under the Montreal Protocol. Our inversion therefore will produce estimates reflecting such reductions. For our emission estimations, we have divided the global industrial source into eight regions: Europe (IND Europe), Northwest Asia (IND NW Asia), South Asia (IND So. Asia), Southeast Asia (IND SE Asia), Africa (IND Africa), Australia/New Zealand (IND Australia), North America (IND N. Amer.), and South America (IND S. Amer.) (Fig. 3). We assume a priori standard errors of ±100% for each region to allow for substantial changes from the reference values (see Table 2). For Australia/New Zealand, analysis of pollution events at the AGAGE stations at Cape Grim, Tasmania and Aspendale, Australia implies a prior of 0.2 ± 0.2 Gg yr^{-1} rather than the larger GDP-based prior of 1.3 ± 1.3 Gg yr^{-1} (P. Fraser, B. Dunse, N. Derek and A. Manning, private communication, 2010). Similar analyses of pollution events at Mace Head, Ireland imply 1996–2004 emissions from the UK, Ireland, France, Germany, Belgium, Netherlands, Luxembourg and Denmark of about 1 Gg yr^{-1} (A. Manning, private communication, 2010). However, this does not include any of the countries of Southern and Eastern Europe, many of which are expected to have large emissions so we retain our GDP-based Europe prior there. Recall that we use monthly average observations that omit pollution events in our inversions, so that our large-scale regional emission estimates are not biased by countries close to the observing stations.

Industrial CCl$_4$ production is expected to be varying in response to the Montreal Protocol and its amendments. Therefore the regional industrial emissions of CCl$_4$ are expected to vary year to year. In consideration of these facts, annual average industrial

emissions in each year of 1996–2004 are estimated, assuming reasonably that there is relatively small variability in emissions within each year.

Oceanic loss for CCl_4 is significant, as noted earlier, and has a partial lifetime of 94 years. Once dissolved in the water, CCl_4 may be removed by chemical reactions,
5   absorption onto particles, and biological consumption (Yvon-Lewis and Butler, 2002). The rate constant for its removal from the atmosphere can be expressed as a function of surface wind speed, temperature, and salinity (Yvon-Lewis and Butler, 2002). Using knowledge of the spatial and temporal distribution of sea surface temperature, salinity, and wind speed over the oceans, and assuming a global mean mole fraction of 103 ppt
10   and a spatially and temporally constant biological degradation rate, Yvon-Lewis and Butler (2002) have computed monthly oceanic uptake rates of CCl_4 distributed over a $2° \times 2°$ grid of the world's oceans. We have converted these maps to the MATCH T42 grids, and scaled them by a constant global factor to reflect an oceanic lifetime of 94 years. The annual average spatial distribution indicates that the uptake rate of CCl_4 per
15   unit area is greatest at mid-latitudes in the NH, resulting from the collocated reasonably warm temperatures and high wind speeds at these latitudes. As noted, these oceanic uptake rates are based on a global average mole fraction of 103 ppt. Since the global mole fraction of CCl_4 is decreasing, the global oceanic sink should be decreasing as well. We also expect intra-annual and interannual variations in the oceanic uptake in
20   response to climatic changes. We therefore estimate the global oceanic sink with a 3-month time resolution for 1996–2004. The global magnitudes of the (a priori) reference fluxes and their roles in the inversion are listed in Table 3. The a priori errors for the state vector elements are taken generously as ±100% of their reference values for the industrial sources and ±50% for the oceanic sink; these easily encompass their
25   uncertainty ranges in the literature.

All of the above emission or sink variables of interest are arrayed in the state vector

in the Kalman filter. This state vector has the form:

$$x = \begin{bmatrix} X_{2004} \\ X_{2003} \\ \ldots \\ X_{1997} \\ X_{1996} \end{bmatrix} \tag{1}$$

For each year k ($k=1996, 1997, \ldots, 2004$), we have the following 12-element sub-vectors:

$$X_k = \begin{bmatrix} x_k^{\text{IND Europe}} \\ x_k^{\text{IND NW Asia}} \\ x_k^{\text{IND So Asia}} \\ x_k^{\text{IND SE Asia}} \\ x_k^{\text{IND Africa}} \\ x_k^{\text{IND Australia}} \\ x_k^{\text{IND N. Amer}} \\ x_k^{\text{IND S. Amer}} \\ x_{k,\text{Winter}}^{\text{Ocean}} \\ x_{k,\text{Spring}}^{\text{Ocean}} \\ x_{k,\text{Summer}}^{\text{Ocean}} \\ x_{k,\text{Fall}}^{\text{Ocean}} \end{bmatrix} \tag{2}$$

These sub-vectors contain the scaling factors for annual industrial flux magnitudes from eight spatial regions and four seasonal oceanic global flux magnitudes. The state vector specifically covers December 1995 to November 2004 (36 seasons in total). Here our definition of annual has a one-month shift from the calendar year in order to be more compliant with the normal definition of a season.

We use the unit pulse method to calculate the sensitivities of the station mole fractions to the state vector elements (Chen and Prinn, 2006). For example, to compute the sensitivities to $x_{1996}^{\text{IND SE Asia}}$, the scaling factor for the 12-month average industrial flux magnitude in SE Asia, a temporally even emission pulse with an intensity of $10\,\text{Gg}\,\text{yr}^{-1}$ over the year 1996 is incorporated and the model is run for two years (1996–1997). Then the semi-normalized sensitivities are deduced by finite differences at a monthly resolution. Because the inter-hemispheric mixing time is around one year and the responses at different sites tend to converge after one year (Xiao et al., 2009), we only conduct a two-year simulation for each pulse. Sensitivities after two years are extrapolated by fitting the decay curves with exponential functions. For the 1996 annual emission pulse from the SE Asian region (Fig. 4), the responses at different sites have different patterns depending on their relative proximity to the source region and on the global time-varying wind fields. Of the stations shown, the Mace Head and Alert stations are located closer to SE Asia in the downwind (westerly) direction, and therefore they respond more rapidly with large response peaks. Taking into account the general circulation patterns, the other three stations are further away from the source region and therefore their responses are delayed with relatively steady and slow increases in their mole fractions followed by decreases due to destruction of CCl$_4$. Note the significant convergence of all five sensitivities after two years as expected.

4 Inversion results

4.1 Forward modeling

Before performing the optimal estimation, we assessed the ability of the a priori emissions and sinks to reproduce the CCl$_4$ observations in a forward run of MATCH. We initialized the atmospheric 3-D distribution of CCl$_4$ using the output from a previous multi-year (1992-1995) run, scaled to fit the observed mole fractions at remote sites such as Alert, Mauna Loa, and Cape Grim during December 1995. These stations

were chosen because they represent better the global background inter-hemispheric gradient due to their long distances from strongly emitting sources. The reference run was then made from December 1995 through August 2005. The monthly mean modeled and observed mole fractions of CCl$_4$ at the indicated stations over the nine-year period of the simulation are compared in Fig. 5. Note the significant differences in the calculated reference (a priori) and observed rates of decrease at most stations. We also note that the reference model simulations have larger seasonal cycles than the observations at Trinidad Head and Mace Head. These modeled seasonal cycles are sensitive to the seasonal variations of the downward flux of CCl$_4$ from the stratosphere to the troposphere. Stratosphere-troposphere exchange (STE) is at a maximum during late winter and early springtime, and is stronger in the NH than in the SH. Because stratospheric CCl$_4$ mole fractions are less than tropospheric mole fractions due to stratospheric photodissociation, the net effect is that the mole fractions of CCl$_4$ at the surface decrease during downward transport episodes. Comparing the model and the observations, we can see that this downward mixing may be overestimated in the MATCH model. Using simulations and observations of ^{14}CO, Jöckel et al. (2002) also concluded that STE in the MATCH model is overestimated. Indeed, when we did trial inversions using 3-month time resolution for industrial sources, the regional industrial emissions showed larger variations in the optimally-estimated emissions than in the reference (and unrealistic differences from expectations about these variations based on knowledge of the CCl$_4$ industry). These differences are simply the responses of the optimized emissions to compensate for the effect of the overestimated downward transport of CCl$_4$. For example, when we looked at the North American region, there were increasing estimated industrial emissions during springtime to compensate for the overestimated decreasing of CCl$_4$ mole fractions from intrusion of stratospheric air. Because of this effect, and because industrial emissions are not expected to vary substantially by season, we estimate 12-monthly average emissions as noted above.

4.2 Industrial emission estimates

In the same period as the reference run, the inversion is conducted by using observations from December 1995 to August 2005. Figure 6 shows the reference and optimized yearly regional industrial source strengths during 1996–2004, with their error bars. Compared to the smooth linearly decreasing reference emissions, the derived emission strengths vary year to year. Substantial decreases in the estimation errors occur, especially for Europe, SE Asia, and North America. However, given the fact that we do not include model transport errors, especially those associated with interannual variations in STE, we cannot be confident that the large inferred interannual changes (e.g. for SE Asia, South Asia) are real. We therefore also show in Fig. 6 the 2-year running average emissions, about which we have greater confidence (these are weighted 2-year averages taking account of the errors (1-sigma) in the proximal 2 years; the reciprocal variances of the 2-year averages are also the sum of the reciprocal variances of the proximal 2 years). Although there is a large difference between optimally estimated and a priori regional CCl_4 emissions, the global total industrial emissions deviate much less from the (a priori) reference. This is expected since the a priori values were themselves derived using atmospheric measurements.

Figure 7 shows the 1996–2004 average optimally estimated industrial emissions and oceanic uptake rates plotted on the global T42 grid of the MATCH model. The dominant roles of SE Asia and South Asia in the global industrial emissions and of the Southern Hemisphere in the global oceanic uptake are very evident.

Figure 8 shows the comparison of the a priori and a posteriori percentage contribution by each region to the global total industrial emissions, averaged for 1996–2004. Recall that the regional contributions for the a priori emissions depended on their GDPs, and the three largest contributions were therefore from North America (38%), SE Asia (36%), and Europe (16%). In contrast, the a posteriori regional contributions reflect the real emissions derived from the measurements, and now we conclude that SE Asia (53%) and South Asia (23%) emitted the largest amounts of CCl_4.

The optimally derived yearly global industrial emissions are compared to the reference emissions and to the emission estimates from industrial sales data (Fig. 2). As expected, the globally aggregated a posteriori emission estimates using the 3-D MATCH model do not differ too much from the a priori 2-D model estimates that were made with a subset of the measurements used here (of course the primary purpose of the 3-D inversions is to provide the regional distribution of CCl$_4$ emissions). Our optimal estimates over the 9-year period indicate a smaller decreasing trend (-0.3 ± 0.6 Gg yr^{-1} per year) in the global CCl$_4$ emissions compared to the reference emissions (-1.4 Gg yr^{-1} per year). Both our optimal and reference emission trends differ very significantly from the very large decrease seen in the industry-based emission estimates. The derived small negative trend in the global emission of CCl$_4$ is consistent with the observed significant negative trend in the global average surface concentration of CCl$_4$, due to the effects of the oceanic and stratospheric sinks.

4.3 Oceanic uptake

As noted earlier, the global oceanic CCl$_4$ uptake rates are solved as seasonal fluxes. Compared to the reference, the optimally estimated oceanic sink is smaller by about 2 Gg yr^{-1} and has a lower amplitude in its annual cycle (Fig. 9). To understand the small seasonal behavior of the global oceanic sink, we note that the oceanic sink (shown as a negative flux) is greatest (more negative) in summer in all four semi-hemispheres (Fig. 10). The oceanic sink in the higher latitude SH (HSH) has the largest seasonal variability, resulting first from the higher winter-to-summer variations in both the NH and SH higher latitudes (HNH and HSH), and second from the larger oceanic area in the HSH. The large seasonal variability in the HSH ocean (Fig. 10) largely determines the small seasonal variability of the global oceanic sink (Fig. 9). The oceanic sink is stronger (more negative) in the tropical regions (LNH and LSH) because of the coincidence of higher temperatures and larger oceanic areas there. The optimized (a posteriori) global oceanic sink retains the phasing but not the magnitude of the seasonal variations of the reference (a priori) sink. The optimized values show modest

interannual variability in the global oceanic uptake rate. Recall that the local oceanic uptake rate is calculated as the uptake rate constant multiplied by the atmospheric mole fraction. Although the uptake rate constant (and the partial lifetime) is independent of the atmospheric burden (Yvon-Lewis and Butler, 2002), the globally decreasing CCl_4 mole fractions lead to a decreasing mass of CCl_4 dissolving in the oceans and being destroyed by subsequent chemical reactions and biological consumption over time; the effect is however small given the $\sim$1% yr^{-1} decrease in mole fractions.

4.4 Global CCl_4 budget

The four terms in the global budget of CCl_4 are shown as a function of time in Fig. 9 with the net loss (negative but shown as a positive number for clarity) being the difference between the industrial emissions and the aggregated stratospheric and oceanic sinks. The seasonal cycle in the stratospheric sink reaches a maximum (i.e., is most negative) in the NH winter, consistent with the winter STE rate being larger in the NH than the SH in the NCEP-driven MATCH model. Since the amplitude of this STE in MATCH is overestimated, the reflections of the STE in the oscillations in the net loss are similarly overestimated. At least in part, this is responsible for the overestimation of the seasonal variations of the mole fractions at some high latitude measurement stations as noted earlier (Fig. 5).

The inversion results have been further aggregated to compute the 9-year average global budget of CCl_4. Figure 11 and Table 2 show the reference and optimally estimated CCl_4 fluxes averaged over the entire period for 1996–2004. Also shown are the optimized errors, which are always less than the reference errors due to the incorporation of the observations into the Kalman filter. The global optimal estimate of the industrial source is 74.1$\pm$4.3 Gg yr^{-1}. Our derived European emission of 3.0$\pm$1.6 Gg yr^{-1} is substantially lower than the reference estimate of 11.8 Gg yr^{-1}, and the North American emission of 4.9$\pm$1.4 Gg yr^{-1} is much less than the 27.7 Gg yr^{-1} reference estimate, presumably because emissions from these regions have been successfully regulated under the Montreal Protocol. Our derived Southeast Asian emission of 39.5$\pm$2.7 Gg yr^{-1}

is higher than the 25.9 Gg yr^{-1} reference, and the second largest source region is South Asia with 16.7±2.2 Gg yr^{-1} emissions. Emissions from other regions are relatively small, and the changes from their reference values (and their error reductions) are also small. Global annual uptake by the oceans during 1996–2004 is ~2 Gg yr^{-1}
5 less than its reference magnitude.

To assess the inversion, we run the forward model with the optimal emission and sink estimates, and compare the residuals between the optimal model and measurements with the residuals for the reference model (Fig. 12). As expected from the application of the Kalman filter to the observational time series, the mole fractions from the run with
10 optimized emissions tend to be much closer to the observations at most of the sites than those from the run with the reference emissions.

5 Conclusions

Using the global 3-D MATCH model and a Kalman filter, we have optimally estimated the annual-average industrial emissions for eight land regions and the seasonal-
15 average (spatially-varying) oceanic sink of CCl$_4$ for each of the nine years from 1996 to 2004.

Overall, there are larger year-to-year variations in the optimally estimated industrial emissions than in the reference emissions (which are simply linearly decreasing). The three regions of Europe, Northwest Asia, and North America show smaller opti-
20 mized emissions relative to their a priori values, which is qualitatively consistent with the emissions from these three regions being regulated under the Montreal Protocol. Our optimally derived South and Southeast Asian emissions are much larger than their reference values indicating growing emissions there. A much smaller negative trend has been derived in the global CCl$_4$ industrial emissions for 1996–2004 compared to
25 those implied from industrial sales data.

The seasonal variability of the global oceanic sink is dominated by the seasonal variability of the HSH oceans, which is greatest in summer and weakest in winter. The

optimized values also show modest interannual variability in the global oceanic uptake rate that is decreasing slowly with time. This decrease is expected because of the globally decreasing CCl$_4$ mole fractions ($\sim$1% yr^{-1}). The seasonal cycle in the global total stratospheric sink peaks in the NH winter consistent with the winter NH STE rate being larger than the winter SH STE rate.

The final errors in the optimal estimate account for errors in the a priori estimates and in the observations (with model-site mismatch errors being incorporated as measurement errors). Other uncertainties in the model that have not been considered, especially transport errors, would increase the derived errors in the a posteriori emission estimates.

Because of the spatial correlation of the hypothesized soil sink for CCl$_4$ with the industrial emissions distribution, and the inconsistency of the measured interhemispheric gradient with the overall CCl$_4$ lifetime of 20 years (which would result from this sink), we do not estimate the soil sink directly in this work. If there is a small soil sink it will simply lower the inferred industrial emissions by that amount.

References

Allen, N. D. C., Bernath, P. F., Boone, C. D., Chipperfield, M. P., Fu, D., Manney, G. L., Oram, D. E., Toon, G. C., and Weisenstein, D. K.: Global carbon tetrachloride distributions obtained from the Atmospheric Chemistry Experiment (ACE), Atmos. Chem. Phys., 9, 7449–7459, doi:10.5194/acp-9-7449-2009, 2009.

Butler, J. H., Battle, M., Bender, M. L., Montzka, S. A., Clarke, A. D., Saltzman, E. S., Sucher, C. M., Severinghaus, J. P., and Elkins, J. W.: A record of atmospheric halocarbons during the twentieth century from polar firn air, Nature, 399, 749–755, 1999.

Chen, Y.-H. and Prinn, R. G.: Estimation of atmospheric methane emissions between 1996 and 2001 using a three-dimensional global chemical transport model, J. Geophys. Res., 111, D10307, doi:10.1029/2005JD006058, 2006.

Clerbaux, C., Cunnold, D. M., Anderson, J., Engel, A., Fraser, P. J., Mahieu, E., Manning, A., Miller, J., Montzka, S. A., Nassar, R., Prinn, R. G., Reimann, S., Rinsland, C. P., Simmonds, P. G., Verdonik, D., Weiss, R. F., Wuebbles, D., Yokouchi, Y.: Chapter 1 Long-lived compounds, in: Scientific Assessment of Ozone Depletion: 2006, Global Ozone Research and Monitoring Project – Report No. 50, World Meteorological Organization, Geneva, Switzerland, 2007.

Cunnold, D. M., Weiss, R. F., Prinn, R. G., Hartley, D. E., Simmonds, P. G., Fraser, P. J., Miller, B. R., Alyea, F. N., and Porter, L.: GAGE/AGAGE measurements indicating reductions in global emissions of CCl_3F and CCl_2F_2 in 1992-1994, J. Geophys. Res., 102(D1), 1259–1269, 1997.

Golombek, A. and Prinn, R. G.: A global three-dimensional model of the circulation and chemistry of $CFCl_3$, CF_2Cl_2, CH_3CCl_3, CCl_4, and N_2O, J. Geophys. Res., 91(D3), 3985–4001, 1986.

Golombek, A. and Prinn, R. G.: Global three-dimensional model calculations of the budgets and present-day atmospheric lifetimes of $CF_2ClCFCl_2$ (CFC-113) and $CHClF_2$ (CFC-22), Geophys. Res. Lett., 16(10), 1153–1156, 1989.

Golombek, A. and Prinn, R. G.: A global three-dimensional model of the stratospheric sulfuric acid layer, J. Atmos. Chem., 16, 179–199, 1993.

Happell, J. D. and Roche, M. P.: Soils: a global sink of atmospheric carbon tetrachloride, Geophys. Res. Lett., 30(2), 1088, doi:10.1029/2002GL015957, 2003.

Jöckel, P., Brenninkmeijer, C. A. M., Lawrence, M. G., Jeuken, A. B. M., and van Velthoven, P. F. J.: Evaluation of stratosphere-troposphere exchange and the hydroxyl radical distribution in three-dimensional global atmospheric models using observations of cosmogenic [14]CO, J. Geophys. Res., 107(D20), 4446, doi:10.1029/2001JD001324, 2002.

Kindler, T. P., Chameides, W. L., Wine, P. H., Cunnold, D. M., Alyea, F. N., and Franklin, J. A.: The fate of atmospheric phosgene and the stratospheric chlorine loadings of its parent compounds: CCl_4, C_2Cl_4, C_2HCl_3, CH_3CCl_3, and $CHCl_3$, J. Geophys. Res., 100(D1), 1235–1251, 1995.

3-D inversion of global CCl$_4$

X. Xiao et al.

Title Page

Abstract	Introduction
Conclusions	References
Tables	Figures

◄◄ ►►

◄ ►

Back Close

Full Screen / Esc

Printer-friendly Version

Interactive Discussion

Krummel, P. B., the AGAGE team and respective participating laboratory investigators: Intercomparison of AGAGE trace gases with other laboratories, unpublished report presented at the 37th meeting of AGAGE scientists, Grindelwald, Switzerland, June 2008, 19 pp., 2008.

Mahowald, N. M.: Development of a 3-dimensional chemical transport model based on observed winds and use in inverse modeling of the source of CCl_3F, PhD thesis, MIT, Cambridge, 1996.

Mahowald, N. M., Rasch, P. J., Eaton, B. E., Whittlestone, S., and Prinn, R. G.: Transport of ^{222}radon to the remote troposphere using the Model of Atmospheric Transport and Chemistry and assimilated winds from ECMWF and the National Center for Environmental Prediction/NCAR, J. Geophys. Res., 102(D23), 28139–28151, 1997a.

Mahowald, N. M., Prinn, R. G., and Rasch, P. J.: Deducing CCl_3F emissions using an inverse method and chemical transport models with assimilated winds, J. Geophys. Res., 102(D23), 28153–28168, 1997b.

Montzka, S. A., Butler, J. H., Meyers, R. C., Thompson, T. M., Swanson, T. H., Clarke, A. D., Locke, L. T., and Elkins, J. W.: Decline in the tropospheric abundance of halogen from halocarbons: Implications for stratospheric ozone depletion, Science, 272, 1318–1322, 1996.

Montzka, S. A., Butler, J. H., Elkins, J. W., Thompson, T. M., Clarke, A. D., and Locke, L. T.: Present and future trends in the atmospheric burden of ozone-depleting halogens, Nature, 398, 690–694, 1999.

Montzka, S. A., Fraser, P. J., Butler, J. H., Connell, P. S., Cunnold, D. M., Daniel, J. S., Derwent, R. G., Lal, S., McCulloch, A., Oram, D. E., Reeves, C. E., Sanhueza, E., Steele, L. P., Velders, G. J. M., Weiss, R. F., and Zander, R. J.: Chapter 1 Controlled substances and other source gases, in: Scientific Assessment of Ozone Depletion: 2002, Global Ozone Research and Monitoring Project – Report No. 47., World Meteorological Organization, Geneva, Switzerland, 2003.

Prinn, R. G., Zander, R., et al.: Chapter 1 Long-lived ozone-related compounds, in: Scientific Assessment of Ozone Depletion: 1998, Global Ozone Research and Monitoring Project – Report No. 44., World Meteorological Organization, Geneva, Switzerland, 1999.

Prinn, R. G.: Measurement equation for trace chemicals in fluids and solution of its inverse, in Inverse Methods in Global Biogeochemical Cycles, Geophys. Monogr. Ser., 114, edited by: Kasibhatla, P., Heimann, M., Rayner, P., et al., AGU, Washington DC, USA, 3–18, 2000.

Prinn, R. G., Weiss, R. F., Fraser, P. J., Simmonds, P. G., Cunnold, D. M., Alyea, F. N., O'Doherty, S., Salameh, P., Miller, B. R., Huang, J., Wang, R. H. J., Hartley, D. E., Harth,

Title Page

Abstract | Introduction

Conclusions | References

Tables | Figures

◄◄ | ►►

◄ | ►

Back | Close

Full Screen / Esc

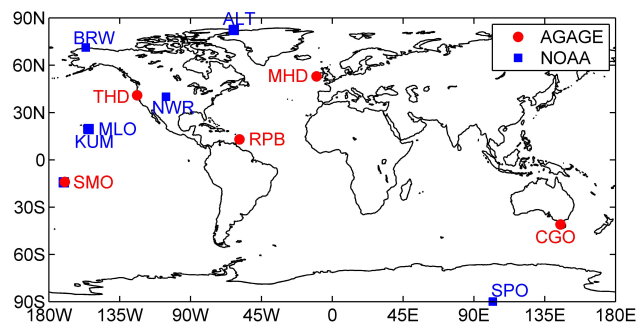Printer-friendly Version

Interactive Discussion

C., Steele, L. P., Sturrock, G., Midgley, P. M., and McCulloch, A.: A histoty of chemically and radiatively important gases in air deduced from ALE/GAGE/AGAGE, J. Geophys. Res., 105(D14), 17751–17792, 2000.

Rasch, P. J., Mahowald, N. M., and Eaton, B. E.: Representations of transport, convection, and the hydrologic cycle in chemical transport models: Implications for the modeling of short-lived and soluble species, J. Geophys. Res., 102(D23), 28127–28138, 1997.

Simmonds, P. G., Cunnold, D. M., Weiss, R. F., Miller, B. R., Prinn, R. G., Fraser, P. J., McCulloch, A., Alyea, F. N., and O'Doherty, S.: Global trends and emission estimates of CCl_4 from in situ background observations from July 1978 to June 1996, J. Geophys. Res., 103(D13), 16017–16027, 1998.

Stohl, A., Seibert, P., Arduini, J., Eckhardt, S., Fraser, P., Greally, B. R., Lunder, C., Maione, M., Mühle, J., O'Doherty, S., Prinn, R. G., Reimann, S., Saito, T., Schmidbauer, N., Simmonds, P. G., Vollmer, M. K., Weiss, R. F., and Yokouchi, Y.: An analytical inversion method for determining regional and global emissions of greenhouse gases: Sensitivity studies and application to halocarbons, Atmos. Chem. Phys., 9, 1597–1620, 2009, http://www.atmos-chem-phys.net/9/1597/2009/.

Volk, C. M., Elkins, J. W., Fahey, D. W., Dutton, G. S., Gilligan, J. M., Loewenstein, M., Podolske, J. R., Chan, K. R., and Gunson, M. R.: Evaluation of source gas lifetimes from stratospheric observations, J. Geophys. Res., 102(D21), 25543–25564, 1997.

Xiao, X., Prinn, R. G., Fraser, P. J., Simmonds, P. G., Weiss, R. F., O'Doherty, S., Miller, B. R., Salameh, P. K., Harth, C. M., Krummel, P. B., Porter, L. W., Mühle, J., Greally, B. R., Cunnold, D., Wang, R., Montzka, S. A., Elkins, J. W., Dutton, G. S., Thompson, T. M., Butler, J. H., Hall, B. D., Reimann, S., Vollmer, M. K., Stordal, F., Lunder, C., Maione, M., Arduini, J., and Yokouchi, Y.: Optimal estimation of the surface fluxes of methyl chloride using a 3-D global chemical transport model, Atmos. Chem. Phys. Discuss., 9, 27693–27744, doi:10.5194/acpd-9-27693-2009, 2009.

Yvon-Lewis, S. A. and Butler, J. H.: Effect of oceanic uptake on atmospheric lifetimes of selected trace gases, J. Geophys. Res., 107(D20), 4414, doi:10.1029/2001JD001267, 2002.

Table 1. Location of the CCl$_4$ measuring stations and their calibration ratios relative to AGAGE (dividing by these ratios places measurements on the AGAGE scale).

Number	ID	Station Location	Latitude	Longitude	Altitude	Laboratory	Calibration
		High Frequency Observations					
1	MHD	Mace Head, Ireland	53.3° N	9.9° W	25	AGAGE	1
2	THD	Trinidad Head, California	41.0° N	124.0° W	140	AGAGE	1
3	RPB	Ragged Point, Barbados	13.0° N	59.0° W	42	AGAGE	1
4	SMO	Cape Matatula, American Samoa	14.3° S	170.6° W	42	AGAGE	1
5	CGO	Cape Grim, Tasmania	41.0° S	145.0° E	94	AGAGE	1
6	BRW	Pt. Barrow, Alaska	71.3° N	156.6° W	8	NOAA	1.0362
7	MLO	Mauna Loa, Hawaii	19.5° N	155.6° W	3397	NOAA	1.0362
8	NWR	Niwot Ridge, Colorado	40.0°N	105.5°W	3018	NOAA	1.0362
9	SMO	Cape Matatula, American Samoa	14.3° S	170.6° W	77	NOAA	1.0362
10	SPO	South Pole, Antarctica	89.9° S	24.8° W	2810	NOAA	1.0362
		Low Frequency Observations					
11	ALT	Alert, Northwest Territories, Canada	82.5° N	62.5° W	210	NOAA	1.0263
12	KUM	Cape Kumukahi, Hawaii	19.5° N	154.8° W	3	NOAA	1.0263

Table 2. Nine-year averaged optimally estimated surface fluxes and their errors for the industrial sources and oceanic sink (units are Gg yr^{-1}). Also shown is the nine-year average stratospheric sink in the forward runs using the reference and optimally estimated industrial emissions and oceanic sink.

Flux type		Reference	Optimization
Industry	Europe	11.8±11.8	3.0±1.6
	NW Asia	2.0±2.0	0.8±1.2
	So Asia	3.0±3.0	16.7±2.2
	SE Asia	25.9±25.9	39.5±2.7
	Africa	1.1±1.1	6.7±0.9
	Australia/NZ	0.2±0.2	0.4±0.2
	N. Amer	27.7±27.7	4.9±1.4
	S. Amer	0.4±0.4	2.0±0.4
	Subtotal	72.1±39.9	74.1±4.3
Oceans		−25.9±12.9	−23.4±5.8
Stratosphere		−70.6	−74.7
Total		−24.4±42.0	−24.0±7.2

Table 3. Reference annual average magnitudes of the sources and sinks of atmospheric CCl$_4$ and their participation in the inversion (Y = yes and N = no).

Source/Sink Type (reference)	Seasonality (Y/N?)	Magnitude (Gg yr^{-1})	In State Vector?
Industry (Cunnold et al., 1997, updated and linearized)	Interannually varying	72 (1996–2004 ave.)	Y (8 regions)
Oceans (Yvon-Lewis and Butler, 2002, scaled)	Y	−26	Y (global)
Soils (Happell and Roche, 2003)	Y	−27	N
Composite	Y	46	–

Fig. 1. Location of CCl$_4$ observing sites used in the inversions (see Table 1 for station abbreviations and inter-calibrations).
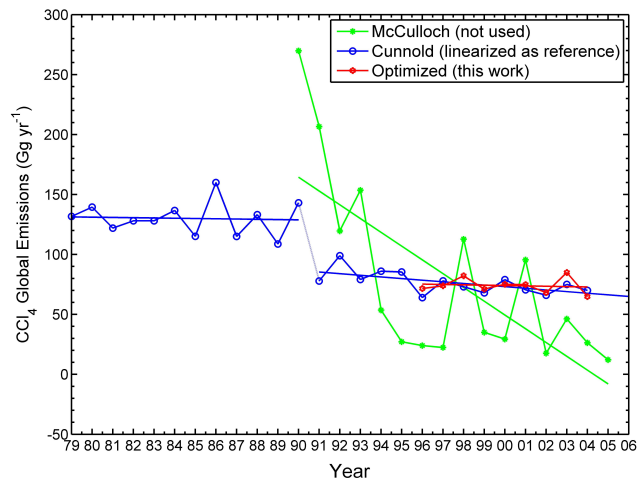
Fig. 2. Yearly global industrial emission estimates from the industrial sales data (McCulloch, private communication, 2009) (green lines) and from the 2-D model inverse modeling approach (Cunnold et al., 1997; Simmonds et al., 1998; updated to 2004) (blue lines), with the corresponding linearly fitted emissions. There are two regimes in the 2-D model emission estimates, and the linearly fitted yearly global emissions for 1996-2004 are used as our reference (a priori) values. Also shown are the a posteriori global annual emission estimates (red lines).

CCl$_4$ Industrial Source Map - Divided Regions
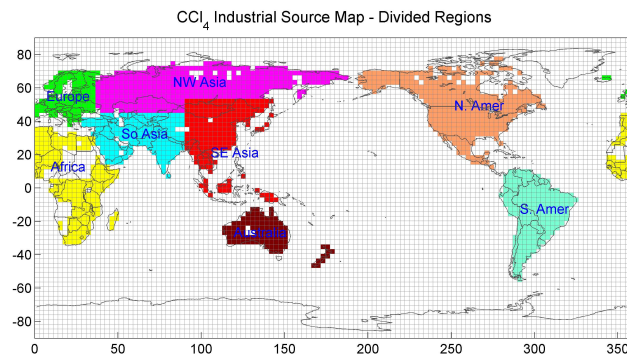
Fig. 3. Partitioning of the global industrial CCl$_4$ source into the eight regions is shown along with the T42 MATCH grids. The regional source magnitudes are estimated in the Kalman filter as 12-month average values. The spatial distributions (but not total emissions) within each source region and for the ocean sink remain at their a priori distributions in the estimation process.
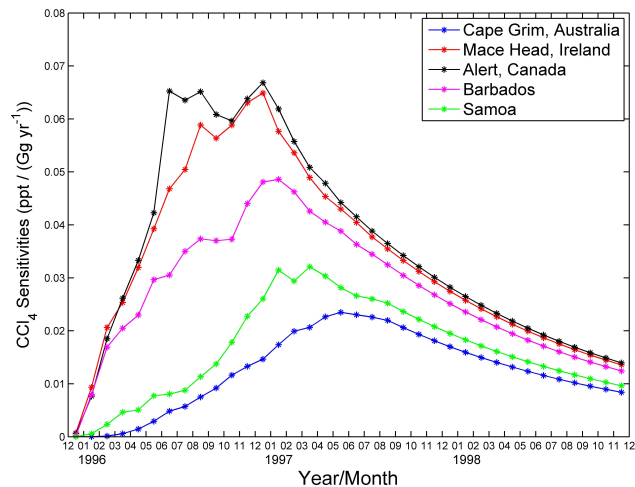
Fig. 4. MATCH-modeled and extrapolated sensitivities of CCl$_4$ mole fractions (ppt) to a 1996 annual emission pulse from the Southeast Asian (SE Asia) industry (Gg yr^{-1}), plotted as monthly means at selected atmospheric measuring stations. The extrapolated sensitivities in this case extend from September 1997 to August 2005, but here only three years of sensitivities are shown.
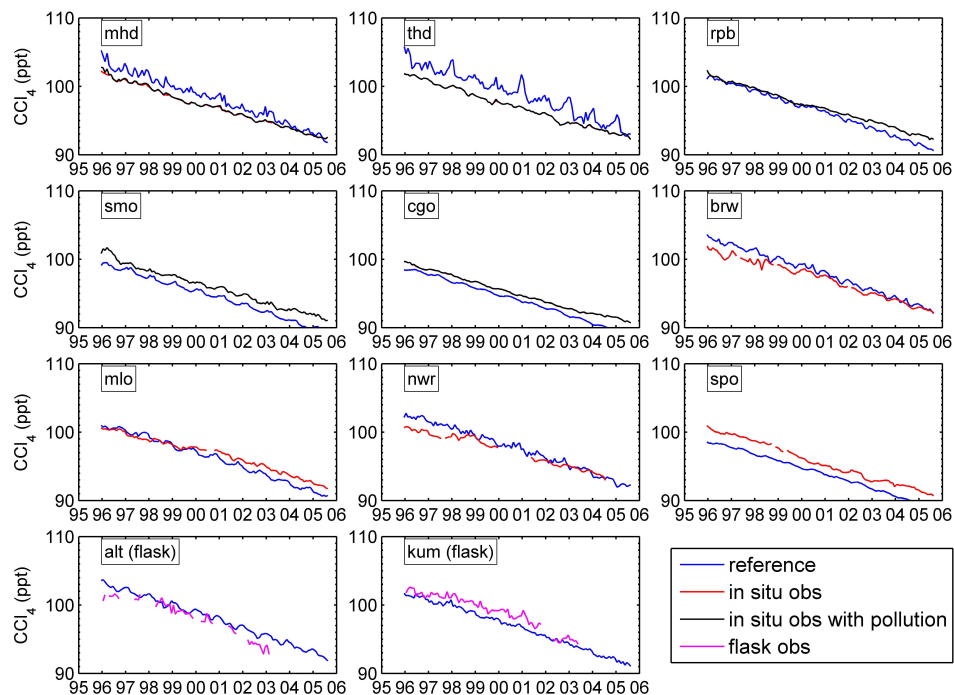
Fig. 5. The time series of the monthly mean CCl$_4$ mole fractions computed in the model using the a priori (reference) surface fluxes (industry source, ocean sink) are compared to the observations. Inclusion of observations that include pollution does not significantly alter the mole fractions on the inversions.
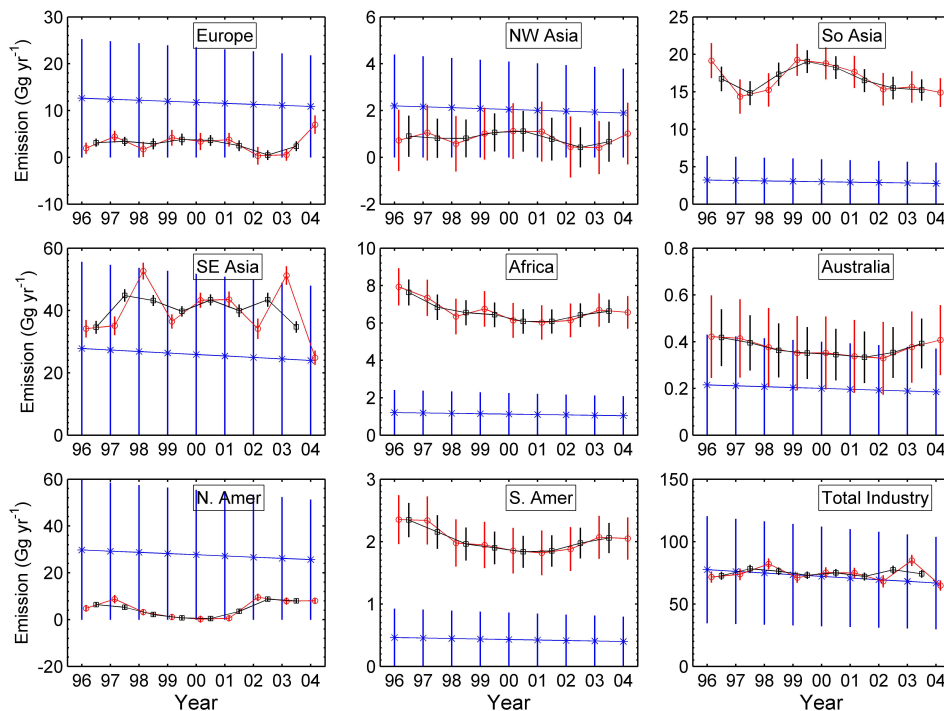
Fig. 6. Inversion results for the 12-month average regional industrial emissions of CCl$_4$. Blue lines show the reference (a priori) magnitudes with error bars, which are assumed to be linearly decreasing. Red lines show the optimized (a posteriori) estimates with error bars (plotted with offset for clarity). Black lines show the 2-year running mean optimized estimates and their errors (see text). The total industry emissions are the sum of the eight regional emissions.
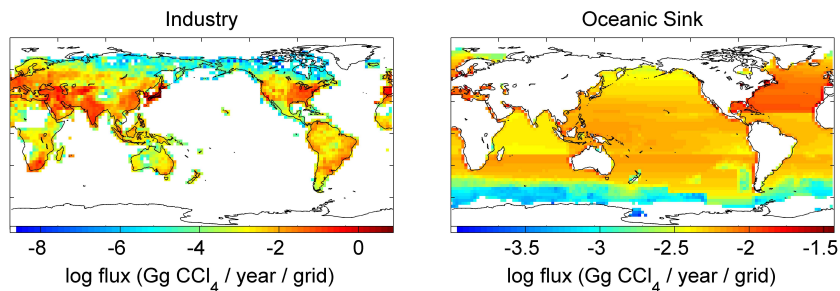
Fig. 7. Optimal annual average distributions of CCl$_4$ industrial emissions (left) and oceanic uptake (right) at each of the MATCH T42 grid points. Oceanic sink magnitudes and spatial patterns vary by month. Global industrial emissions have been divided into eight regions whose total annual emission magnitudes are estimated individually. The magnitude of the oceanic sink is estimated on a 3-month time scale and a global spatial scale as a multiplier on the above monthly varying global sink patterns.

(a) A priori Emissions

S. Amer.: < 1%
Europe: 16%
NW Asia: 3%
So Asia: 4%
N. Amer.: 38%
SE Asia: 36%
Australia: < 1%
Africa: 2%

(b) A posteriori Emissions

Europe: 4%   S. Amer.: 3%
NW Asia: 1%
N. Amer.: 7%
Australia: < 1%
Africa: 9%
So Asia: 23%
SE Asia: 53%
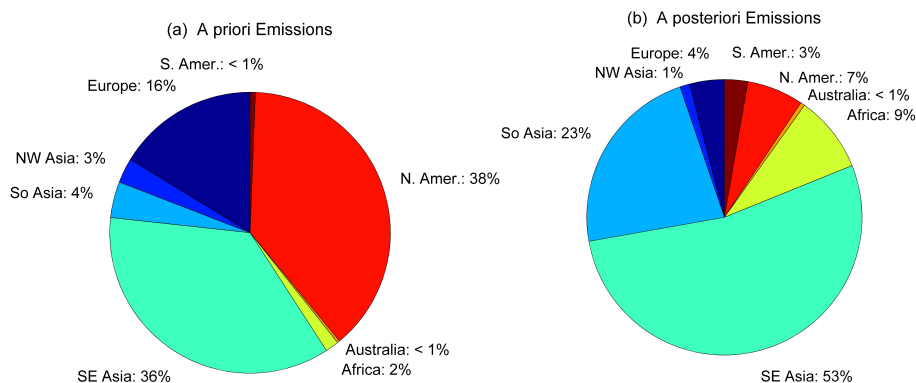
Fig. 8. A priori **(a)** and a posteriori **(b)** regional contributions to the global industrial emissions of CCl$_4$.
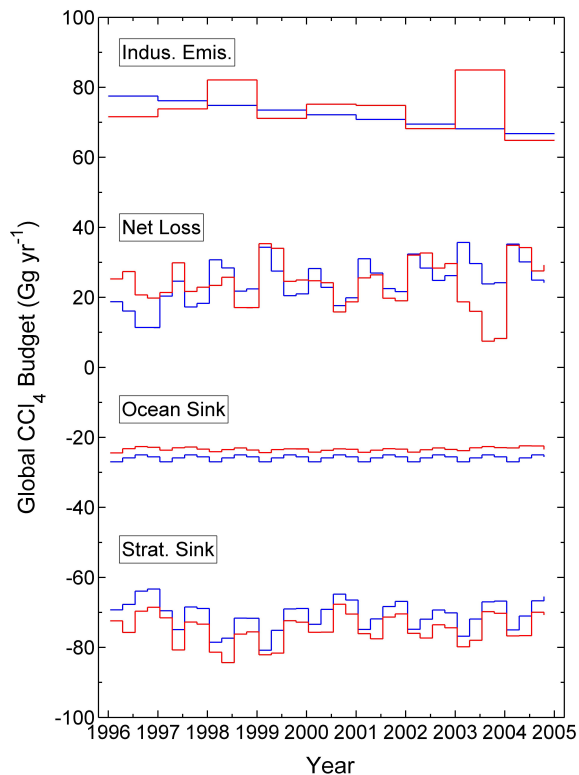
Fig. 9. Global budget of CCl$_4$ over the 1996–2004 period. The blue lines show the reference and the red lines show the optimization (error bars are not shown but are given in Figs. 6 and 11 and Table 2). Global industrial emissions, oceanic sink, and stratospheric sink are shown at one year, 3-month, and 3-month time intervals, respectively. Note that the net loss is actually negative in magnitude, but here the absolute values are shown to avoid overlapping with the coincidentally similar-valued oceanic sink.
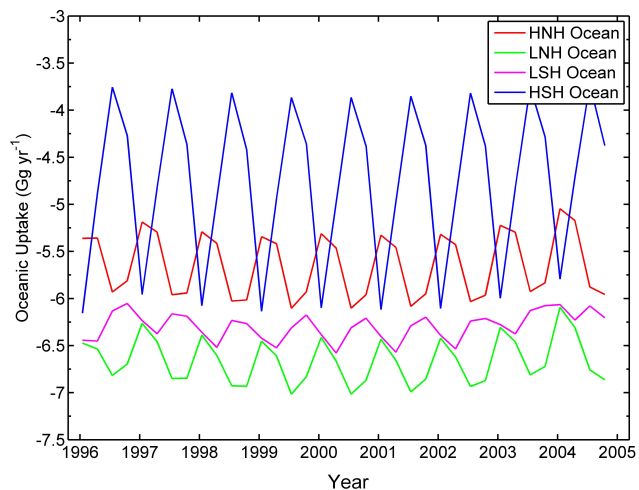
Fig. 10. Seasonal cycles of the optimally estimated semi-hemispheric oceanic sinks (negative fluxes) of CCl$_4$. Note the dominance of the tropical sinks (most negative). Oceanic uptake in the HSH has the largest seasonal variation. Note that the breakdown into semi-hemispheres uses the imposed sink patterns (see Fig. 7).
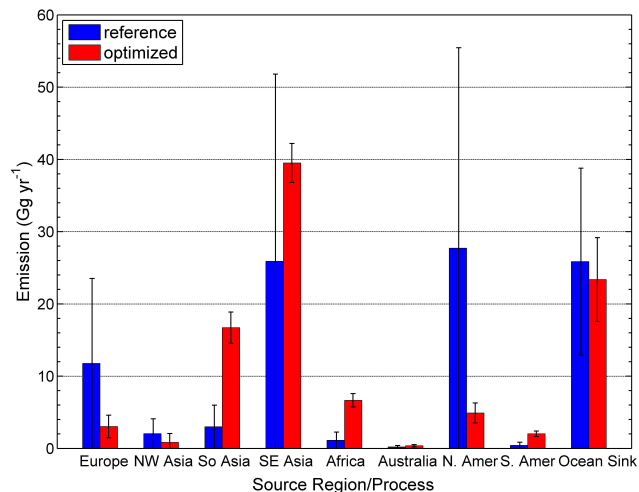
Fig. 11. Annual average magnitudes of the surface fluxes (eight regional emissions and global oceanic sink) of CCl$_4$. Shown are the reference (blue bars) and optimized (red bars) values with their 1-σ error bars. The errors on the reference values are derived from the assumed a priori inversion uncertainties.
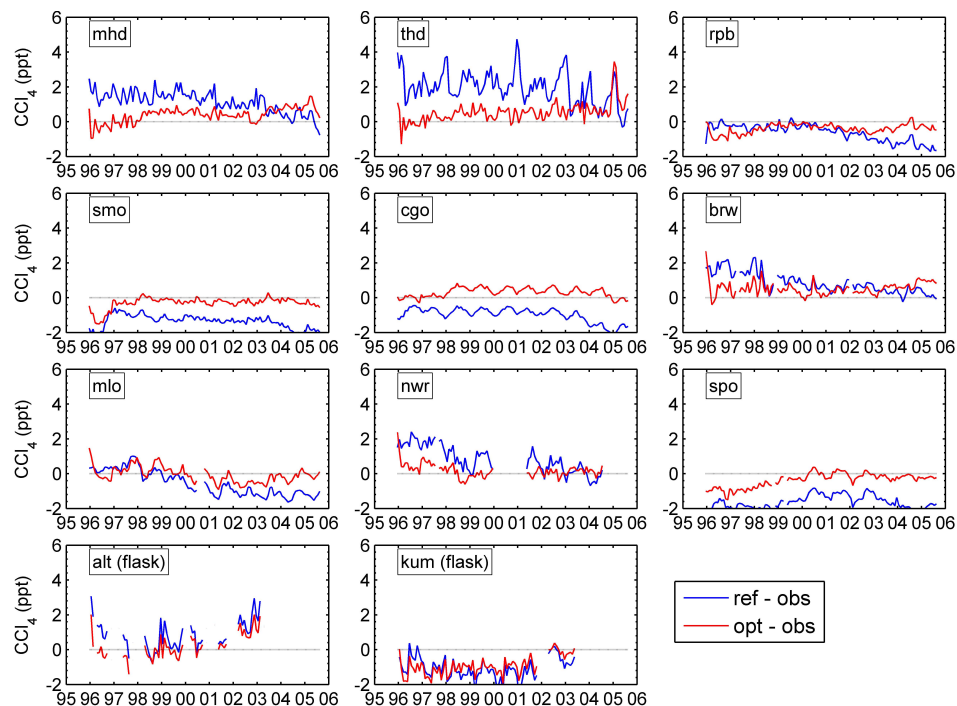
Fig. 12. Residuals between the optimized and observed monthly mean mole fractions of CCl$_4$ (red lines), compared to the residuals between the reference and observed monthly mean mole fractions (blue lines) at each observing site.